J Solid State Electrochem (2009) 13:1433–1440
DOI 10.1007/s10008-008-0692-2

ORIGINAL PAPER

Fabrication of modified TiO_2 nanoparticle carbon paste electrode for simultaneous determination of dopamine, uric acid, and L-cysteine

M. Mazloum Ardakani · A. Talebi · H. Naeimi · M. Nejati Barzoky · N. Taghavinia

Received: 8 July 2008 / Revised: 22 August 2008 / Accepted: 26 September 2008 / Published online: 25 October 2008
© Springer-Verlag 2008

Abstract A carbon paste electrode, modified with 2, 2′-[1,7-hepthandiylbis(nitriloethylidyne)]-bis-hydroquinone and TiO_2 nanoparticles, was used for the simultaneous determination of dopamine (DA), uric acid (UA), and L-cysteine. The study was carried out by using cyclic voltammetry, chronoamperometry, and square wave voltammetry (SWV) techniques. Some kinetic parameters such as the electron transfer coefficient (α) and heterogeneous rate constant (k_s) were also determined for the DA oxidation. A dynamic range of 8.0–1400 μM, with the detection limit of 8.4×10^{-7} M for DA, was obtained using SWV (pH=7.0). The prepared electrode was successfully applied for the determination of DA, UA, and L-cysteine in real samples.

Keywords Carbon paste electrode · Dopamine · Uric acid · L-Cysteine · Nanoparticles

Introduction

Various carbon-based electrodes such as glassy carbon and carbon paste electrodes (CPE) are commonly employed in electrochemical applications due to their excellent properties. These properties include low background currents and the wide potential range. On the other hand, the electron transfer rates, observed at carbon electrodes, are often slower than those observed at metal surfaces [1]. The usual approach in overcoming the slow kinetics at carbon electrodes is the modification of electrode surface with a chemical modifier [2–4]. In this regard, the incorporation of metal nanoparticles on carbon and even the metal electrodes has been suggested in recent years in order to enhance the electron transfer rate. The unique electronic, optical, and catalytic properties of metal and semiconductor nanoparticles (1–200 nm), together with the different methods available for the preparation of nanoparticles of controlled shape and size, provide exciting building blocks for the nanoscale assemblies, structures, and devices. The conjugation of nanoparticles with biomaterials is a tempting research project that provides a route into nanobiotechnology. Evolution has optimized the fascinating macromolecular structures, which exhibit unique recognition, transport, and catalytic properties. The conjugation of nanoparticles with biomaterials could provide electronic or optical transduction of the biological phenomena. In general, there are four main advantages to the use of a nanoparticle-modified electrode as compared to a macroelectrode: high effective surface area, effective mass transport, catalysis, and the control over local microenvironment [5]. Thus, the metal nanoparticle-modified electrodes are increasingly used in many electrochemical applications. The large surface-to-volume ratio and active sites of these nanosized metal particles, in electrocatalysis, constitute a part of the driving force in developing the nanosized electrocatalysts. Electrocatalytic properties of nanoparticle-modified electrodes depend on the important factors such as the nature of substrate, crystalline surface structure, size, and the local microenvironment of nanoparticles. Unlike bulk films, metal nanoparticles exhibit an unusual property of quantized double-layer

M. M. Ardakani (✉) · A. Talebi
Department of Chemistry, Yazd University,
Yazd 89195-741, Iran
e-mail: mazloum@yazduni.ac.ir

H. Naeimi · M. N. Barzoky
Department of Chemistry, University of Kashan,
Kashan 87317, Iran

N. Taghavinia
Nanoparticles and Coatings Lab, Department of Physics,
Sharif University of Technology,
Tehran 14588, Iran

charging effects. However, relatively little work has been carried out to date to elucidate the electrochemical behavior of metal nanoparticles. It is evident from electrochemical, photochemical, and spectroelectrochemical experiments that metal nanoparticles possess a unique property of storing electrons [6].

Dopamine (DA) was discovered to be an important neurotransmitter of mammalian central nervous system during the late 1950s and is found in high amounts (50 nmol/g) in a region of brain, known as the "caudate nucleus" [7]. The very low concentration of DA in the "extracellular fluid" of the caudate nucleus provides a large challenge for the detection of DA. It was also found that Parkinson's disease patients show an almost complete depletion of DA within this region. A major problem in DA determination is the resolution between DA and the coexisting species such as uric acid (UA) and L-cysteine (CySH). At the traditional solid electrodes, UA and CySH are oxidized at the potentials close to DA, resulting in an overlapping voltammetric response [8–10].

In general, a complex structure is designed toward a particular end, perhaps to facilitate an electrode process or to inhibit a reaction or to produce selectivity toward a particular process. The end is achieved by developing within the structure a favorable interplay of the dynamics by which electrons are conveyed between the electrode and the species whose oxidation or reduction is ultimately required to achieve the goal. It may be necessary to employ a selective catalyst or to restrict access to the interior of the structure or to allow for the ready flow of electrons to more remote parts of an assembly [11]. During the present study (with attention to the previous studies [12–14]), we report the electrochemical behavior of DA at the surface of 2,2′-[1,7-hepthandiylbis (nitriloethylidyne)]-bis-hydroquinone (HBNBH; Scheme 1) and TiO_2 nanoparticle-based carbon paste electrode. In addition, we have discussed the suitability of this modified electrode for the voltammetric determination of DA, UA, and CySH in an aqueous solution by square wave voltammetry (SWV).

Experimental

Chemicals

DA, UA, CySH, titanium tetraisopropoxide, H_2O_2, graphite fine powder, and viscous paraffin were obtained from Merck (Darmstadt, Germany) and used as received. All other chemicals used in this investigation were of analytical grade. All solutions were prepared with double-distilled water. The buffer solution (0.1 M) was prepared with H_3PO_4 and the pH was adjusted with the help of 2.0 M NaOH. DA, UA, and CySH solutions were freshly prepared just prior to use and all the experiments were carried out at the ambient laboratory temperature (approximately 25 °C). TiO_2 nanoparticles were synthesized in our laboratory. Colloidal suspension of TiO_2 nanoparticles was synthesized by mixing titanium tetraisopropoxide, H_2O_2, and H_2O with volume proportions of 12:90:200, respectively. The resulting solution was refluxed for 10 h to promote the crystallinity (surface area=84 m^2 g^{-1} and particle size=6.7 nm).

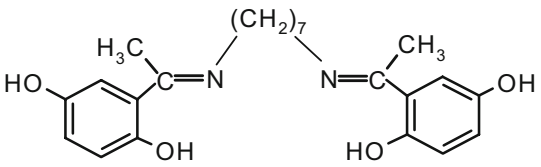

Scheme 1 2, 2′-[1,7-hepthandiylbis(nitriloethylidyne)]-bis-hydroquinone

Synthesis of 2,2′-[(1,7-heptanediylbis(nitriloethylidine)]-bis-hydroquinone

To a mixture of 2,5-dihydroxyacetophenone (0.3 g, 2 mmol) in methanol, 1,7-diaminoheptane (0.13 g, 1 mmol) was added by stirring in one portion. The mixture stirring was continued up to 1 h. The reaction progress was monitored by thin-layer chromatography. After the reaction completion, a yellow substance was precipitated. The solid product was filtered and washed off with the cold methanol. The obtained crude product was recrystallized in methanol and the 2,2′-[(1,7-heptanediylbis(nitriloethylidine)]-bis-hydroquinone, with m.p. 218–219 °C, was obtained as the yellow crystals in 98% yield.

2,2′-[(1,7-heptanediylbis(nitriloethylidine)]-bis-hydroquinone; yellow solid, m.p: 218–219 °C

Infrared (KBr)/ν (cm^{-1}) 3,400–3,500 (br, OH), 3,042, 2,950 (s), 2,800, 2,600, 1,619 (s, C=N), 1,550, 1,390 (s, ArC=C), 1,450, 1,300, 1,225 (s, C–O), 860 (s), 800 (s), 500 (m).

^{1}H nuclear magnetic resonance (NMR; 400 MHz/dimethyl sulfoxide (DMSO))/δ ppm 1.2 (m, 6 H, 3 CH_2), 1.45 (m, 4 H, 2 CH_2), 2.01 (s, 6 H, 2 CH_3), 3.3 (t, 4 H, 2 CH_2), 6.41 (d, 2 H, Ar), 6.53 (d d, 2 H, Ar), 6.77 (d, 2 H, Ar), 8.6 (br, 2 H, 2 OH), 15.3 (s, 2 H, 2 OH).

^{13}C NMR (100 MHz/DMSO)/δ ppm 15.95, 28.44, 30.16, 31.62, 50.43, 115.16, 119.6, 120.6, 121.6, 149.6, 157.1, 173.0.

Apparatus and procedures

All of the electrochemical experiments were carried out using a Sama 500 potentiostat (Isfahan, Iran).The experimental cell was equipped with the modified CPE as a working electrode, a platinum electrode as an auxiliary electrode, and a saturated calomel electrode as a reference. All of the potentials were quoted versus this reference electrode. A personal computer

was used for the data storage and processing. Modified carbon paste was prepared in a conventional fashion by the thorough hand mixing of HBNBH (5.0 mg), TiO_2 nanoparticle (20.0 mg), graphite powder (500 mg), and paraffin oil (86.0 mg) in a pestle mortar. The modified carbon paste was packed into the glass hole of the electrode body and leveled off with a spatula. Contact was made with a copper wire through the center of the rod, screwed to the device. The pH was measured with a Metrohm model 691-pH/mV meter.

Results and discussion

Voltammetric behaviors of the modified TiO_2 nanoparticles carbon paste electrode

The plots of the anodic peak currents, as a function of potential sweep rate, are shown in Fig. 1A. The electrochemical responses of the HBNBH-modified TiO_2 nanoparticles carbon paste electrode (MTNCPE) were those anticipated for a bulk-modified redox couple because the peak currents were directly proportional to the scan rate (Fig. 1A), as predicted for a diffusionless system.

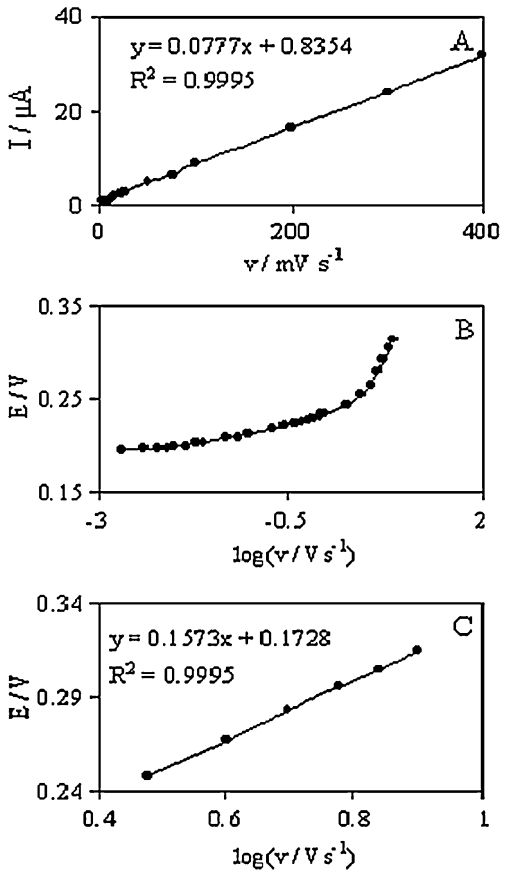

Fig. 1 **A** The dependence of peak currents on the scan rate of MTNCPE. **B** Variation of E_p versus the logarithm of MTNCPE scan rate. **C** Magnification of the same plot for high scan rates

An approximate estimate of the electrode-surface coverage was made by adopting the method used by Sharp et al. [15]. According to this method, the peak current is related to the surface concentration of electroactive species (Γ) by the following equation:

$$I_p = n^2F^2A\Gamma\upsilon/4RT \quad (1)$$

Where n represents the number of electrons involved in the reaction; A is the surface area (0.0962 cm^2) of the modified carbon paste electrode (MCPE); Γ (mol cm^{-2}) is the surface coverage and other symbols have their usual meanings. From the slope of anodic peak currents versus scan rate (Fig. 1A), the calculated surface coverage of HBNBH-modified CPE was 2.1×10^{-10} mol cm^{-2} for n=2. The heterogeneous charge transfer rate constant (k_s) and the charge transfer coefficient (α) of a bulk-modified redox couple can be evaluated by cyclic voltammetric experiments and the variation of anodic peak potentials with scan rate, according to the procedure of Laviron [16]. Figure 1A shows the variations of peak potentials (E_p) as a function of potential scan rate. The present experiment showed that, for scan rates higher than 1,000 mV s^{-1}, the E_p values are proportional to the logarithm of scan rate (Fig. 1C). Under these conditions, the following equation can be used to determine the electron transfer rate constant between HBNBH and CPE [16]:

$$\log k_s = a\log(1-a) + (1-a)\log a - \log(RT/nF\upsilon) - a(1-a)\left(n_aF\,\Delta E_p/2.3RT\right) \quad (2)$$

Where $(1-\alpha)n_a = 0.38$ (see below), n=2, $\Delta E_p = E_{p.a} - E_{p.c}$; ν is the sweep rate and all other symbols have their conventional meanings. From the values of ΔE_p, corresponding to different sweep rates, an average value of k_s was found to be 25.24±0.38 s^{-1}. Also, from the slopes of Fig. 1C plots, the average value of the charge transfer coefficient was found to be 0.62.

Effects of pH

Generally, the electrode process of HBNBH involves the participation of protons. The effect of pH on the MTNCPE signal was investigated by differential pulse voltammetry using 0.1 M buffer solutions with various pH values ranging from 2.0 to 12.0. In all the cases, the ionic strength was adjusted to 0.1 M. As can be demonstrated by Fig. 2, the formal potential ($E_{1/2}$) of MTNCPE was pH dependent. One linear segment was found with slope values of 51 mV/pH. The redox reactions of quinone derivatives occur with the participation of two electrons [17–18]. The total number of protons, which also participate in the redox process of HBNBH, may vary in accordance with the pH range. Depending on the number of protons taking part in the redox process with two-electron transfer, the $E_{1/2}$ shifts by

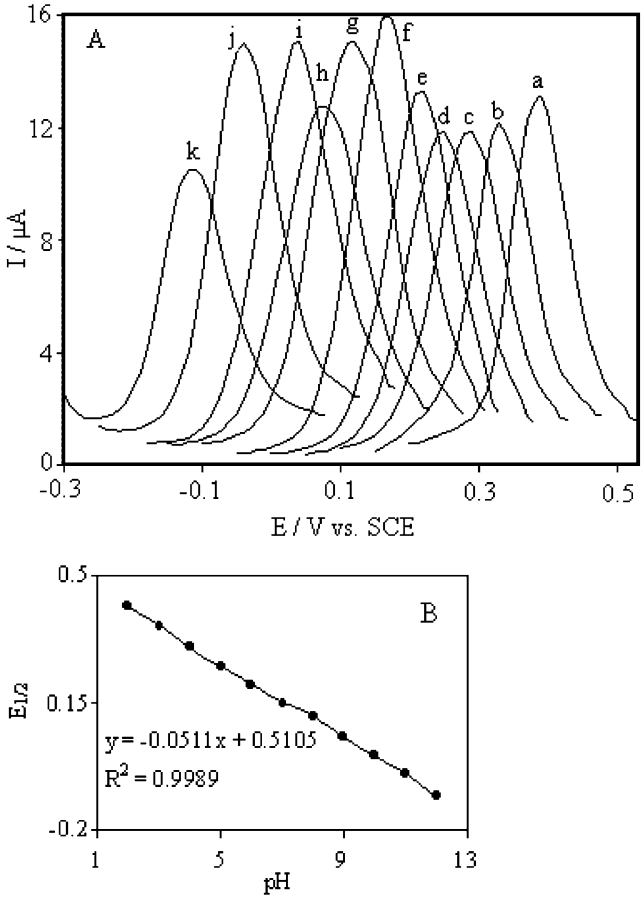

Fig. 2 **A** Differential pulse voltammograms of MTNCPE at various pHs. **B** Dependence of the half wave potential ($E_{1/2}$) of MTNCPE on the pH

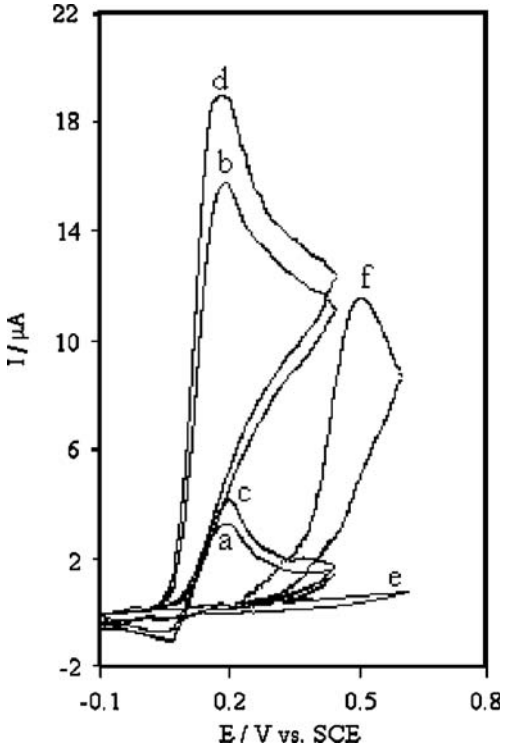

Fig. 3 Cyclic voltammograms of: (*a*) modified carbon paste electrode in 0.1 M phosphate buffer (pH 7.0) solution, (*b*) the same electrode in 0.5 mM DA solution (pH 7.0), (*c*) MTNCPE in the buffer, (*d*) the same electrode in 0.5 mM DA solution (pH 7.0), (*e*) unmodified CPE in buffer, and (*f*) the same electrode in 0.5 mM DA solution (pH 7.0). The scan rate was 25 mV s^{-1} during all the cases

−59.2 mV/pH ($2H^+$), −29.6 mV/pH ($1H^+$), and 0.0 mV/pH (without H^+) [11]. So, there are two protons, transferred during the redox reaction, in the pH range of 2.0–12.0. Figure 2B demonstrates that the pH 7.0 gave the best shape and the highest current.

Electrochemistry of DA at MTNCPE

In order to test the potential electrocatalytic activity of the MTNCPE, its cyclic voltammetric responses were obtained in phosphate buffer (pH 7.0) at 25 mV s^{-1}, in the presence and absence of 0.5 mM DA (Fig. 3). In the absence of DA, a peak of MCPE could be observed (Fig. 3, curve a). Upon the addition of 0.5 mM DA, there was a drastic enhancement of the anodic peak current, and, in addition, no cathodic current was observed in the reverse scan (Fig. 3, curve b). With the addition of TiO_2 (nanoparticle) to MCPE, a remarkable increase in current was observed in the absence of DA (Fig. 3, curve c) and in the presence of 0.5 mM DA (Fig. 3, curve d). This behavior is consistent with a very strong electrocatalytic effect. Under the same experimental conditions, the direct oxidation of DA at an unmodified carbon paste electrode shows an irreversible wave at more positive potentials (Fig. 3, curve f). The catalytic peak potential was found to be about 182 mV, whereas the uncatalyzed-peak potential was recorded to be about 450 mV. Thus, a decrease in the overvoltage of approximately 268 mV and an enhancement of the peak current were also achieved with the modified electrode. Table 1 compares some modified electrodes used in the electrocatalysis of dopamine.

Effect of scan rate

The scan rate dependence of cyclic voltammograms of the MTNCPE, in 0.1 M phosphate buffer solution containing 1.0 mM DA, is presented in Fig. 4. Inset a shows that a plot of the catalytic peak current versus the square root of the sweep rate is linear, suggesting that, at sufficient overpotential, the reaction is diffusion-limited. A plot of the sweep rate normalized current ($I_p/\nu^{1/2}$) versus sweep rate (inset b) exhibits the characteristic shape, typical of an EC_{cat} process. Andrieux and Savéant [19] developed a theoretical model for such a mechanism and derived a relationship between the peak current and the substrate

Table 1 Comparison of some modified electrodes used in the electrocatalysis of dopamine

Substrate	pH	Linear range/μM	Detection limit	E_{pa}/mV[a]	E_{pa}/mV[b]	Peak potential shift/mV	Ref.
MCPE[c]	5.0	1.0–100.0	5.0×10^{-7}	_	_	_	[23]
CILE[d]	6.8	2.0–1,500.0	1.0×10^{-6}	345 vs. Ag/AgCl	210 vs. Ag/AgCl	135 vs. Ag/AgCl	[24]
MCPE[c]	6.0	200.0–950.0	1.5×10^{-5}	380 vs. Ag/AgCl	285 vs. Ag/AgCl	95 vs. Ag/AgCl	[25]
MCPE[c]	7.0	8.0–1,400.0	8.4×10^{-7}	450 vs. SCE	182 vs. SCE	268 vs. SCE	This work

[a] Ascorbic acid peak potential at the surface of unmodified electrode
[b] Ascorbic acid peak potential at the surface of modified electrode
[c] Modified carbon paste electrode
[d] Carbon ionic liquid electrode

concentration for the case of a slow rate (ν) and a large catalytic rate constant (k'_h):

$$I_{cat} = 0.496nFAC_s\upsilon^{1/2}(nFD/RT)^{1/2} \quad (3)$$

Where D and C_s are the diffusion coefficient ($cm^2\ s^{-1}$) and the bulk concentration (mol cm^{-3}) of the substrate (DA in this case), respectively. Low values of k'_h result in the values lower than 0.496 for the constant. Based on extensive computations, a working is given, which shows the relationship between numerical values of the constant, $I_{cat}/nFAc_s(DnF\nu/RT)^{1/2}$ and $\log\left[k'_h\Gamma\Big/(DnF\upsilon/RT)^{1/2}\right]$ (Fig. 1 of [19]). The value of k'_h can thus be calculated from such a working curve. For low scan rates (2–30 mV s^{-1}), we have found the value of this constant to be 0.3 for an MTNCPE with a coverage of $\Gamma=2.1\times10^{-10}$ mol cm^{-2}, a geometric area (A) of 0.0962 cm^2, and considering the $D=8.2\times10^{-6}$ $cm^2\ s^{-1}$ (which is obtained by chronoamperometry as stated below), in the presence of 1.0 mM DA. Using this value and Fig. 1 from the theoretical paper by Andrieux and Savéant [19], the values of k'_h were found to be 1.96×10^{-3}, 2.26×10^{-3}, and 2.53×10^{-3} for the scan rates of 6, 8, and 10 mV s^{-1}. These values better explain the sharp feature of the catalytic peak, observed for catalytic oxidation of DA at the MTNCPE. The number of electrons in the overall reaction can also be obtained from the slope of the I_p versus $\nu^{1/2}$ plot (Fig. 4, inset a). Using the slope of this plot and according to the following equation for a totally irreversible diffusion-controlled process [20]

$$I_p = 3.01\times10^5[(1-a)n_a]^{1/2}AC_sD^{1/2}\upsilon^{1/2} \quad (4)$$

and considering $(1-\alpha)n_\alpha=0.64$ (see below), it is estimated that the total number of electrons involved in the anodic oxidation of DA is $n=2$. A Tafel plot is a useful device for evaluating the kinetic parameters. Inset c of Fig. 4 shows the Tafel plot, drawn by using the data derived from the rising part of the current–voltage curve at a scan rate of 25 mV s^{-1}. The number of electrons involved in the rate-determining step (n_α) and the exchange current density (j_0) can be estimated from the slope and the intercept, respectively, of the Tafel plot [11]. A Tafel slope of 10.838 V per decade was obtained, indicating that a one-electron process was involved in the rate-determining step, assuming a charge transfer coefficient of $\alpha=0.36$. Also, the value of j_0 was found to be 0.54 μA cm^{-2} from the intercept of the Tafel plot.

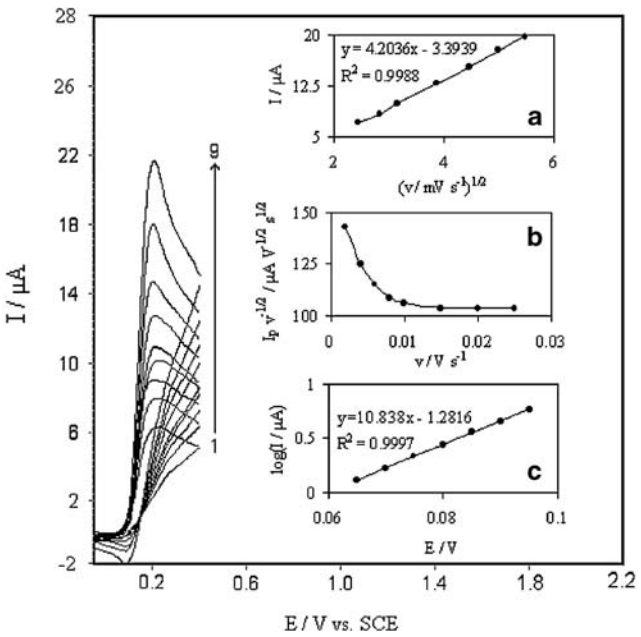

Fig. 4 Cyclic voltammograms of a MTNCPE in 0.1-M phosphate buffer (pH 7.0) containing 1.0 mM DA at different scan rates. The *numbers 1–9* correspond to 2, 4, 6, 8, 10, 15, 20, 25, and 30-mV s^{-1} scan rates, respectively. *Insets*: (*a*) variation of the electrocatalytic currents versus the square root of scan rate, (*b*) variation of the scan rate normalized current ($I_p/v^{1/2}$) with scan rate. (*c*) Tafel plot, derived from the current potential curve, recorded at the scan rate of 25 mV s^{-1}

Chronoamperometry

The catalytic oxidation of DA, by an MTNCPE, was also studied by chronoamperometry. Chronoamperograms, obtained at a potential step of 500 mV, are depicted in Fig. 5. In chronoamperometric studies, we have determined the diffusion coefficient of DA for an MTNCPE. Figure 5 (inset A) shows the experimental plots of I versus $t^{-1/2}$ with the best fits for different concentrations of DA employed. The slopes of the resulting straight lines were then plotted

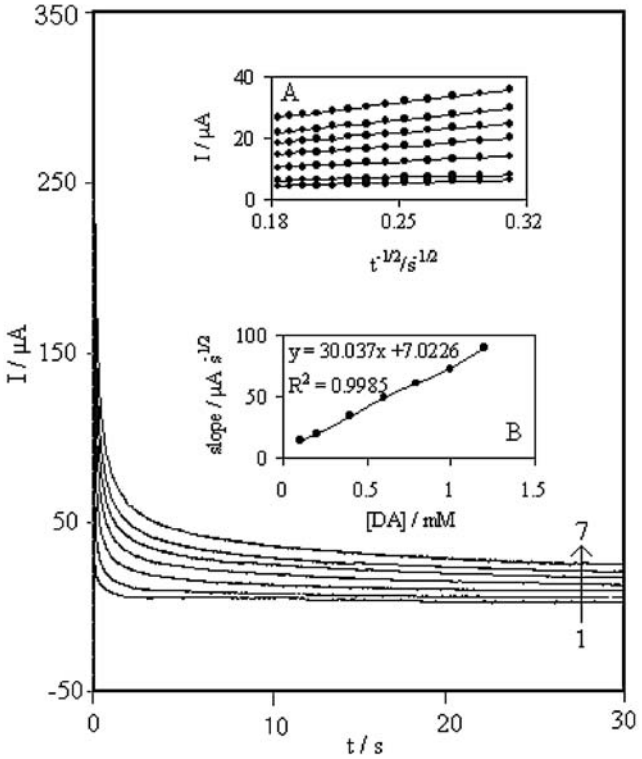

Fig. 5 Chronoamperometric response of MTNCPE in 0.1 M phosphate buffer (pH 7.0) at a potential step of 500 mV for different concentrations of DA. The *numbers 1–7* correspond to 0.1, 0.2, 0.4, 0.6, 0.8, 1.0, and 1.2 mM. *Insets*: (*A*) Plots of *I* versus $t^{-1/2}$ obtained from chronoamperograms, (*B*) plot of the slope of straight lines against the DA concentration

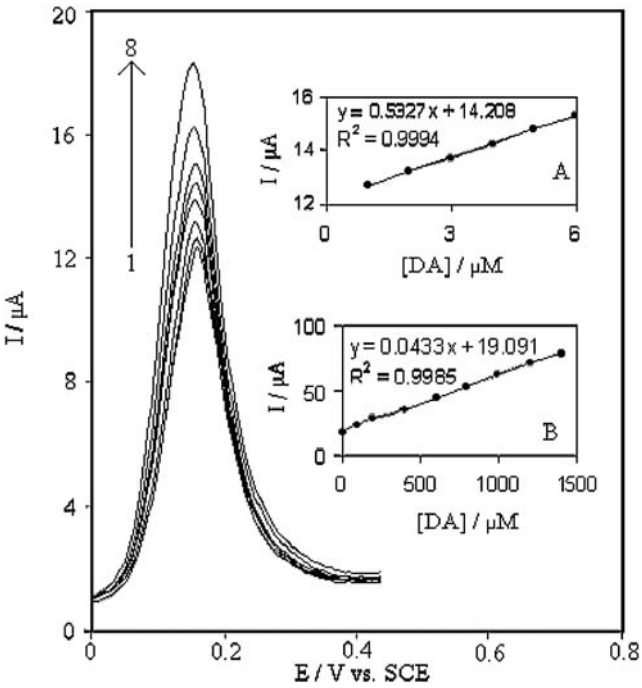

Fig. 6 Square wave voltammograms of MTNCPE in 0.1 M phosphate buffer solution (pH 7.0) containing different concentrations of DA (from inner to outer): 1.0, 2.0, 4.0, 6.0, 8.0, 10.0, 20.0, and 40.0 μM. *Insets* show the plots of the electrocatalytic peak current as a function of DA concentration in the range of: (*A*) 1.0 to 6.0 μM and (*B*) 8.0 to 1400 μM

versus the DA concentration (Fig. 5, inset B). By using the slopes and the Cottrell equation [11], we have calculated the diffusion coefficient of 8.2×10^{-6} cm^2 s^{-1} for DA, although the calculated value of the diffusion coefficient is in good agreement with the values reported by others [21].

Calibration curve and the detection limit

For the determination of detection limit for DA, SWV technique was employed. Since SWV has a much higher current sensitivity and better resolution than cyclic voltammetry, it was used to estimate the lower detection limit and simultaneous determination of DA, UA, and CySH. In addition, the charging current contribution to the background current that is a limiting factor in the analytical determination is negligible in SWV mode. Figure 6 shows the SWVs obtained for the oxidation of different DA concentrations at the MTNCPE. Figure 6 (insets A and B) demonstrates clearly that the plot of peak current versus DA concentration is constituted of two linear segments with different slopes, corresponding to two different ranges of substrate concentration. The decrease of sensitivity (slope) in the second linear range (Fig. 6, inset B) is likely to be due to kinetic limitation. From the analysis of these data, we estimate that the lower detection limit of DA is of the order of 0.84 μM according to the definition $Y_{LOD}=Y_B+3\sigma_B$ [22].

Simultaneous determination of DA, UA, and CySH at MTNCPE

One of the main objectives of this study was the development of a modified electrode capable of the electrocatalytic oxidation of DA and the separation of electrochemical responses for DA, UA, and CySH. Using MTNCPE as the working electrode, the analytical experiments were carried out either by varying the UA or the CySH concentration in the presence of 100 μM DA in 0.1 M phosphate buffer (pH 7.0). Figure 7A shows SWVs obtained with increasing concentrations of CySH in the presence of 100.0 μM DA. Figure 7B shows the SWVs obtained with increasing concentrations of UA in the presence of 100 μM DA. In the case of the MTNCPE, two well-defined oxidation peaks of DA–CySH or DA–UA mixtures were observed. As shown in Fig. 7, an increase in the peak current of CySH was observed with the increasing CySH concentration and the SWV peak of DA was almost unchanged during the CySH oxidation. It can also be noted from these results that the responses to DA, CySH, and UA, at the MTNCPE, are relatively independent. The utilization of the MTNCPE for the simultaneous determination of DA, CySH, and UA was

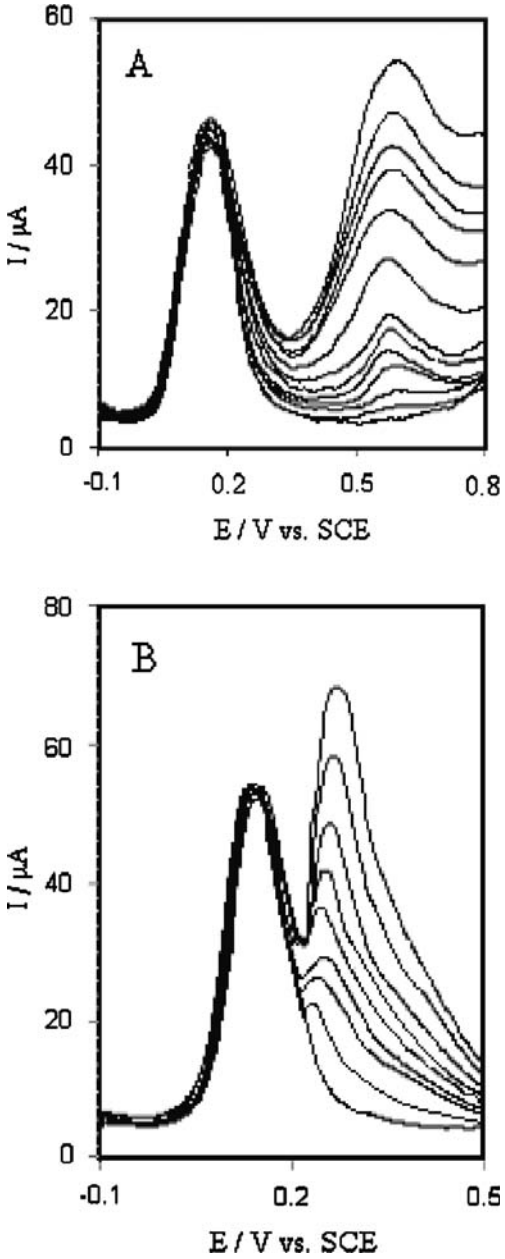

Fig. 7 **A** Square wave voltammograms of MTNCPE in 0.1 M phosphate buffer solution (pH 7.0) containing 100 μM DA and different concentrations of CySH (from inner to outer): 0.0, 10, 20, 40, 60, 80, 100, 200, 400, 600, 800, 1,000, and 2,000 μM. **B** Square wave voltammograms of MTNCPE in 0.1 M phosphate buffer solution (pH 7.0) containing 100 μM DA and different concentrations of UA (from inner to outer): 0.0, 10, 20, 40, 60, 80, 100, 120, and 140 μM

demonstrated by simultaneously changing the DA, CySH, and UA concentrations. The SWV results show that the simultaneous determination of DA, CySH, and UA, with three well-distinguished anodic peaks at the potentials of 155, 345, and 574 mV, is possible at the modified electrode, which corresponds to the oxidation of DA, UA, and CySH, respectively. Figure 8 shows the linear ranges of CySH and UA concentrations, estimated to be 180–1,000 μM

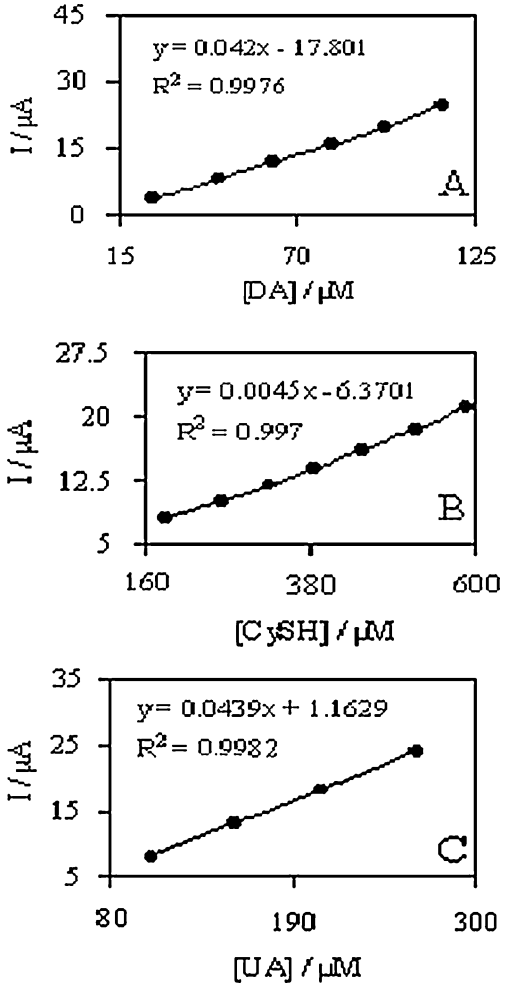

Fig. 8 Plots of the peak currents as a function of concentration of: **A** DA in the range 20–120 μM, **B** CySH in the range 180–600 μM, and **C** UA in the range 100–270 μM

(Fig. 8B) and 100–600 μM (Fig. 8C), respectively. The obtained peak current increased linearly with the increasing concentration of DA. The sensitivities of modified electrode towards the oxidation of CySH and UA were found to be 0.0045 and 0.0439 μA μM^{-1}, respectively. Whereas, the electrode sensitivities towards DA were found to be

Table 2 Results of recovery of the spiked DA to 10.0 mL of the dilute (fivefold) dopamine ampoule sample

No.	Amount of added DA standard solution (mg)	Amount of found[a] DA (mg)	Recovery (%)
1	–	0.398	–
2	0.152	0.545	99.1
3	0.265	0.671	101.2
4	0.364	0.785	103.0
5	0.455	0.838	98.2
6	0.607	1.001	99.6

[a] RSD for five replications in the spiked range of DA concentration was less than 4.0%

0.0433 μA μM^{-1} in the absence of CySH and UA while 0.042 μA μM^{-1} in the presence of CySH and UA. It is interesting to note that the sensitivities of the modified electrode, towards DA, in the absence and presence of CySH and UA are virtually the same, which indicates the fact that the oxidation processes of DA, CySH, and UA occur independently at the MTNCPE. Therefore, the simultaneous or independent measurements of the three analytes are possible without any interference. If the DA signal is affected by CySH or UA, the above-mentioned slopes would be different.

Determination of DA in dopamine ampoule

The modified electrode, incorporated with the HBNBH, was successfully applied for DA measurements in the pharmaceutical preparations (dopamine ampoules). One milliliter of the dopamine ampoule was diluted to 50 mL with a phosphate buffer solution (0.1 M, pH=7.0); then, 0.5 mL of this solution was diluted to 10 mL and transferred to the voltammetric cell for the SWV determination at MTNCPE. The diluted ampoule sample was spiked with various concentrations of standard DA solution (4.0×10^{-3} M) and its SWVs were obtained by MTNCPE. This procedure was repeated five times and the recovery was between 96.2% and 105.7% (Table 2).

Conclusions

The present study has indicated that the MTNCPE exhibits good electrocatalytic activity towards the DA oxidation. The electrochemical behavior of the modified electrode is strongly dependent on solution pH. The electron transfer coefficient (α) and the average heterogeneous catalytic reaction rate constant (k'_h) for DA oxidation, at the MTNCPE, were also determined as 0.36 and 2.25×10^{-3} cm s^{-1}, respectively. The diffusion coefficient of DA was calculated to be 8.2×10^{-6} cm^2 s^{-1} for the experimental conditions, using chronoamperometric results. Finally, the MTNCPE can simultaneously detect DA, UA, and CySH, which coexist in a homogeneous solution and the separation of the oxidation peak potentials are about 190 and 419 mV for DA–UA and the DA–CySH, respectively.

Acknowledgements The authors wish to thank the Yazd University Research Council, the IUT Research Council, and the Excellence in Sensors for their financial supports to the present work.

References

1. McCreery RL (1991) In: Bard AJ (ed) Electroanalytical chemistry. vol. 17. Dekker, New York, pp 221–374
2. Durst RA, Baumner AJ, Murray RW, Buck RP, Andrieux CP (1997) Pure Appl Chem 69:1317. doi:10.1351/pac199769061317
3. Kutner W, Wang J, L'Her M, Buck RB (1998) Pure Appl Chem 70:1301. doi:10.1351/pac199870061301
4. Murray RW, Ewing RW, Durst RA (1987) Anal Chem 59:379A. doi:10.1021/ac00132a001
5. Katz E, Willner I, Wang J (2004) Electroanalysis 16:19. doi:10.1002/elan.200302930
6. Rao CNR, Müller A, Cheetham AK (2004) The chemistry of nanomaterials, synthesis, properties and applications. Wiley, New York
7. Wightman RM, May LJ, Michael AC (1988) Anal Chem 60:769A. doi:10.1021/ac00164a001
8. Gonon F, Buda M, Cespuglio R, Jouvet M, Pujol JF (1980) Nature 286:902. doi:10.1038/286902a0
9. O'Neill RD (1994) A review. Analyst 119:767. doi:10.1039/an9941900767
10. Salimi A, Mam-Khezri H, Hallaj R (2006) Talanta 70:823. doi:10.1016/j.talanta.2006.02.015
11. Bard AJ Faulkner LR (2001) Electrochemical methods, fundamentals and applications. Wiley, New York
12. Beitollahi H, Mazloum Ardakani M, Naeimi H, Ganjipour B (2008) J Solid State Electrochem (in press)
13. Mazloum Ardakani M, Ebrahimi Karami P, Rahimi P, Zare HR, Naeimi H (2007) Electrochim Acta 52:6118. doi:10.1016/j.electacta.2007.03.065
14. Mazloum Ardakani M, Akrami Z, Kazemian H, Zare HR (2006) J Electroanal Chem 586:31. doi:0.1016/j.jelechem.2005.09.015
15. Sharp M, Petersson M, Edstrom K (1979) J Electroanal Chem 95:123. doi:10.1016/S0022-0728(79)80227-2
16. Laviron E (1979) J Electroanal Chem 101:19. doi:10.1016/S0022-0728(79)80075-3
17. Golabi SM, Zare HR (1999) Electroanalysis 11:1293. doi:10.1002/(SICI)1521-4109(199911)11:17<1293::AID-ELAN1293>3.0.CO;2-2
18. Raoof J, Ojani R, Ramine M (2007) Electroanalysis 19:597. doi:10.1002/elan.200603760
19. Andrieux CP, Savéant JM (1978) J Electroanal Chem 93:163. doi:10.1016/S0022-0728(78)80230-7
20. Antoniadou S, Jannakoudakis AD, Theodoridou E (1989) Synth Met 30:295. doi:10.1016/0379-6779(89)90652-8
21. Moreno G, Pariente F, Lorenzo E (2000) Anal Chim Acta 420:29. doi:10.1016/S0003-2670(00)01011-4
22. Miller JN, Miller JC (2000) Statistics and chemometrics for analytical chemistry, 4th edn. Pearson Education Ltd., Harlow
23. Shahrokhian S, Zare-Mehrjardi HR (2007) Sens Actuators B Chem 121:530. doi:10.1016/j.snb.2006.04.088
24. Safavi A, Maleki N, Moradlou O, Tajabadi F (2006) Anal Biochem 359:224. doi:10.1016/j.ab.2006.09.008
25. Raoof JB, Ojani R, Rashid-Nadimi S (2005) Electrochim Acta 50:4694. doi:10.1016/j.electacta.2005.03.002